Accepted Manuscript

Pyromellitic dianhydride-based polyimide anodes for sodium-ion batteries

Qinglan Zhao, Rohit Ranganathan Gaddam, Dongfang Yang, Ekaterina Strounina, Andrew K. Whittaker, X.S. Zhao

PII: S0013-4686(18)30276-7

DOI: 10.1016/j.electacta.2018.01.208

Reference: EA 31190

To appear in: *Electrochimica Acta*

Received Date: 12 September 2017

Revised Date: 4 January 2018

Accepted Date: 31 January 2018

Please cite this article as: Q. Zhao, R.R. Gaddam, D. Yang, E. Strounina, A.K. Whittaker, X.S. Zhao, Pyromellitic dianhydride-based polyimide anodes for sodium-ion batteries, *Electrochimica Acta* (2018), doi: 10.1016/j.electacta.2018.01.208.

Graphical abstract

Pyromellitic dianhydride-based polyimides $[C_{16}H_6O_4N_2]_n$ with different crystallinity and morphology were synthesised by simple one-step hydrothermal method. The electrochemical performance and sodium storage mechanism of the polyimide-based organic electrode as anode for sodium-ion batteries were investigated.

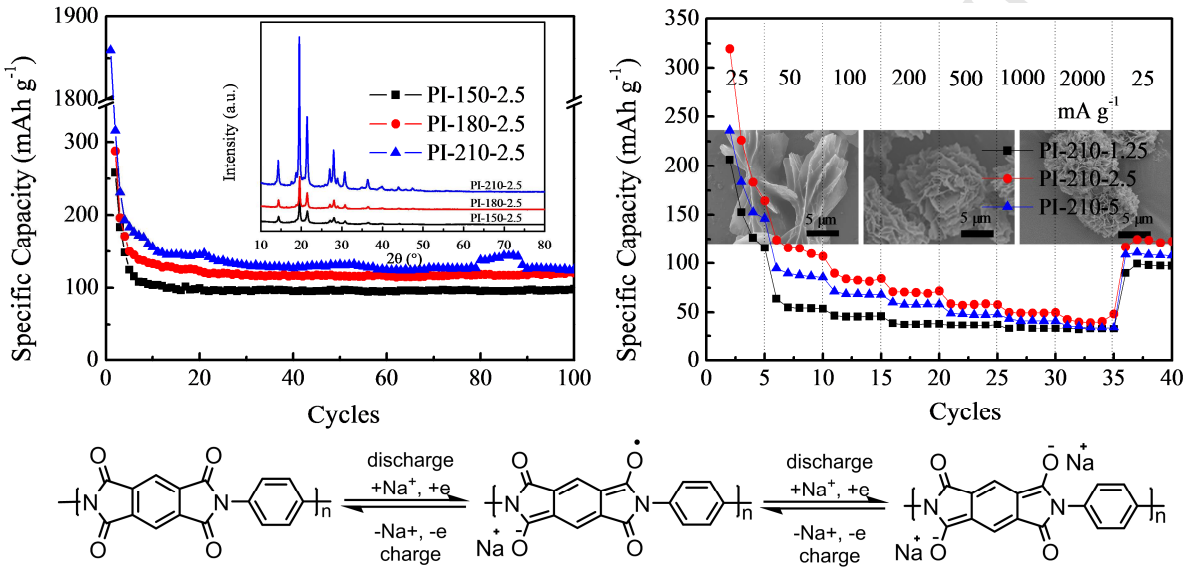

Pyromellitic dianhydride-based polyimide anodes for sodium-ion batteries

Qinglan Zhao[a], Rohit Ranganathan Gaddam[a], Dongfang Yang[a], Ekaterina Strounina[b], Andrew K. Whittaker[c], and X. S. Zhao[a*]

[a] School of Chemical Engineering, The University of Queensland, St Lucia, QLD 4072, Australia

[b] Centre for Advanced Imaging, The University of Queensland, QLD 4072, Australia

[c] Australian Institute for Bioengineering and Nanotechnology, The University of Queensland, St. Lucia QLD 4072, Australia

[*]Corresponding author E-mail address: george.zhao@uq.edu.au

Abstract

Organic redox-reactive polymers have garnered great attention as a promising alternative for conventional transition-metal compounds in sodium-ion batteries (NIBs) due to their low cost, structural flexibility and diverse structure. Among this class of materials, polyimides with high mechanical strength, excellent thermal stability and high density of electroactive functional groups have shown promise as low-cost electrode materials for NIBs. Herein, a simple hydrothermal method was used to synthesise pyromellitic dianhydride-based polyimides $[C_{16}H_6O_4N_2]_n$. The polyimides consisting of interconnected nanosheets with a microflower-like morphology were tested as an NIB anode. The polyimide electrode exhibited a stable discharge capacity of 125 mAh g^{-1} at a current density of 25 mA g^{-1} at the 100^{th} cycle. At a high current density of 2 A g^{-1}, the electrode delivered a discharge capacity of 43 mAh g^{-1}. The capacity contribution of this polyimide electrode mainly occurred below 1.5V making it suitable as an organic NIB anode. The mechanism of sodiation and

desodiation during discharge and charge was studied using Fourier transform infrared spectroscopy, in which this polyimide experienced two-step enolisation reaction with reversible insertion of two sodium ions during the redox electrochemical reaction.

Keywords

Polyimide; Polymer; Organic electrode; Sodium-ion battery; Anode

1. Introduction

Sodium-ion batteries (NIBs) have attracted a great attention as an alternative to lithium-ion batteries (LIBs) due to the limited natural occurrence of lithium,[1-3] higher abundance and lower cost of sodium resources (the cost of Na_2CO_3 is only 3 % of that of Li_2CO_3)[4, 5] as well as the similar electrochemical properties of sodium and lithium (sodium is only 0.3 V more positive than lithium).[6]

Although many cathode materials suitable for NIBs have been identified, the choice for anode materials is however very limited.[7-12] The most commonly used anode in LIBs, graphite, is unfortunately not suitable for NIBs because it hardly allows sodium intercalate into the space between the graphene layers, and the intercalation is electrochemically irreversible.[13] The current leading anode candidate, hard carbon, can exhibit stable cycling performance but poor rate capability, due to its rigid tortuous nanometric structure.[14] Transition-metal inorganic compounds are extensively studied as anode materials for NIBs. However, due to their limited mineral resources, concerns over recyclability and environmental issues warrant cheap and alternative electrode materials. Also, large sodium ions inserting into the rigid lattices can cause multi-step phase transitions, which can lead to low utilisation of capacity and/or sluggish kinetics.[15]

Organic materials stand out in the energy storage field as promising alternatives to inorganic compounds because of their flexibility, easy processability and structural and compositional diversity.[16, 17] For example, polyimides with high mechanical strength, excellent thermal stability and high density of electroactive functional groups are promising redox-active electrode materials for rechargeable batteries.[18, 19] Aromatic carbonyl-derivative polyimides, containing a dianhydride core as the aromatic backbone, have been commonly used as cathodes for NIBs.[20-22] However, recently it was found that when altering the aromatic core from perylene 3,4,9,10-tetracarboxylic dianhydride (PTCDA) to 1,4,5,8-naphthalenetetracarboxylic dianhydride (NTCDA) and to pyromellitic dianhydride (PMDA), the average discharge voltage became progressively lower.[23] For the PMDA-based polyimide, the average discharge voltage was only approximately 1.73 V, indicating its potential suitability as an anode material for NIBs due to its relatively low voltage (< 2 V vs. Na/Na^+).[13]

Current research on organic electrodes is mainly concerned with the molecular design of different organic materials. In fact, structure and morphology also play an important role in the electrochemical performance of the organic electrodes. Recently it was found that disodium terephthalate with nanosheet-like morphology exhibited much improved electrochemical properties than the bulk spheroidal morphology.[1] However, such studies on the effects of structure and morphology on a certain organic material are very infrequently reported.

Here, we report the electrochemical behaviour of a PMDA-based polyimide as an organic anode in sodium-ion batteries. The effects of the structure and morphology on the electrochemical performance of polyimides were investigated by controlling the synthesis temperature and reagent concentrations. The mechanism of sodium storage in the organic electrode material indicates a two-step enolisation reaction with reversible insertion of two

sodium ions. The nontoxic polyimide is cheap and easy to synthesise, possibly fulfilling the needs for large-scale battery applications.

2. Experimental section

2.1 Synthesis of pyromellitic dianhydride-based polyimides

2.5 mmol p-phenylenediamine (PPD) was dissolved in 30.0 mL N,N-dimethylformamide (DMF) followed by adding equimolar PMDA under stirring at room temperature. The mixture was then transferred into a Teflon lined autoclave and hydrothermally treated at 150, 180 or 210 °C for 10 h. The precipitate was separated by centrifugation, washed with DMF and ethanol several times, and dried under vacuum at 80 °C for 24 h. The as-synthesised samples are defined as PI-150-2.5, PI-180-2.5 and PI-210-2.5, where PI stands for polyimide, 150, 180 and 210 indicate the synthesis temperature, and 2.5 is the concentration of the PPD and PMDA added in millimoles per litre. The as-synthesised samples PI-150-2.5, PI-180-2.5 and PI-210-2.5 were heated at 100, 200 and 300 °C for 1 h under vacuum, respectively for post curing (PC). Samples thus obtained are named by adding the prefix PC before a sample, for example, PC-PI-150-2.5. Other polyimide samples were also synthesised with different concentrations of PPD and PMDA using the same method as described above under the hydrothermal treatment temperature of 210 °C. Samples thus obtained are designated as PI-210-1.25, PI-210-2.5 and PI-210-5.

2.2 Characterisation

Fourier transform infrared (FTIR) spectra of powder samples were recorded on an attenuated total reflectance FTIR (ATR-FTIR) spectrometer (Nicolet 5700, Thermo Electron). ^{13}C magic angle spinning nuclear magnetic resonance (MAS NMR) spectra were acquired on a Bruker Avance III spectrometer at a ^{13}C Larmor frequency of 75.468 MHz. All the experiments were carried out with a Bruker 4 mm MAS probe and zirconia rotor spinning at 5 kHz. A CPMAS

pulse sequence was used with 100 kHz decoupling and a 3 s relaxation delay. X-ray diffraction (XRD) measurements were performed on an X-ray diffractometer (Bruker D8 Advance, Bruker) with Cu Kα radiation (λ = 1.54056 Å). The morphology of the samples was characterised using a field emission scanning electron microscope (FESEM) (JSM-7100F, JEOL). Nitrogen adsorption-desorption measurements were carried out on a surface area and pore size analyser (TriStar II 3020, Micromeritics) at 77 K. The specific surface area (S_{BET}) and pore size distribution were analysed by the Brunauer-Emmett-Teller (BET) and Barrett-Joyner-Halenda (BJH) methods, respectively. The total pore volume (V_t) was estimated at the relative pressure of 0.99, micropore volume (V_{mic}) was obtained using the t-plot method, and the mesopore volume (V_{meso}) was calculated from the difference between V_t and V_{mic}.

2.3 Electrochemical measurements

Polyimide, carbon black, and poly(vinylidene difluoride) (PVDF) were dispersed in N-methyl pyrrolidone (NMP) at a mass ratio of 6:3:1 to form a slurry, which was casted onto a copper foil current collector using a doctor blade. The electrode was dried at 60 °C under vacuum for 12 h. A coin cell was assembled in an Argon-filled glovebox using the polyimide electrode as the working electrode, pure sodium foil as the counter electrode, glass fibre as the separator and 1 mol L^{-1} $NaClO_4$ in equal volume of ethylene carbonate (EC) and propylene carbonate (PC) mixed with 0.3 wt % fluoroethylene carbonate (FEC) as the electrolyte.

Galvanostatic discharge and charge cycling were conducted on a battery tester (CT3008, Neware) at room temperature. Cyclic voltammetry (CV) measurements were carried out on an electrochemical workstation (CHI 660D, Chen Hua Instrument). To study the mechanism of charging, the charged or discharged electrodes were obtained from dissembled coin cells composed of polyimide as the positive electrode and sodium metal as the negative electrode, washed with anhydrous dimethyl carbonate (DMC) and then dried

naturally in the glove box for characterisations. The theoretical capacity was calculated based on a two-electron transfer redox process for each formula unit using the following equation:[16]

$$C(\mathrm{mAhg^{-1}}) = \frac{n \times F\left(\mathrm{Cmol^{-1}}\right)}{M_w\left(\mathrm{gmol^{-1}}\right)} = \frac{n \times 96485(\mathrm{C})}{M_w(\mathrm{g})} = \frac{n \times 96485(\mathrm{As})}{M_w(\mathrm{g})} = \frac{n \times 96485 \times 1000/3600(\mathrm{mAh})}{M_w(\mathrm{g})} = \frac{26801 \times n}{M_w}\left(\mathrm{mAhg^{-1}}\right) \quad (1)$$

C, n, F and M_w are the theoretical specific capacity, the transferred electron number in each formula unit (here n = 2), the Faraday constant and the molecular weight of the formula unit, respectively.

3. Results and discussion

Fig. 1a shows the FTIR spectra of the as-synthesised samples PI-150-2.5, PI-180-2.5 and PI-210-2.5 prepared at different hydrothermal temperatures. All characteristic absorbance signals of the imide group can be seen. The peaks at 1782, 1720 and 723 cm^{-1} can be assigned to the asymmetric stretching vibration (ν_{as}), symmetric stretching vibration (ν_s) and bending vibration (δ) of the imide group C=O, respectively. The peak at 1380 cm^{-1} can be assigned to the stretching vibration of the imide C–N group. The FTIR results are in good agreement with previously reported data,[23] demonstrating the successful synthesis of the polyimide.

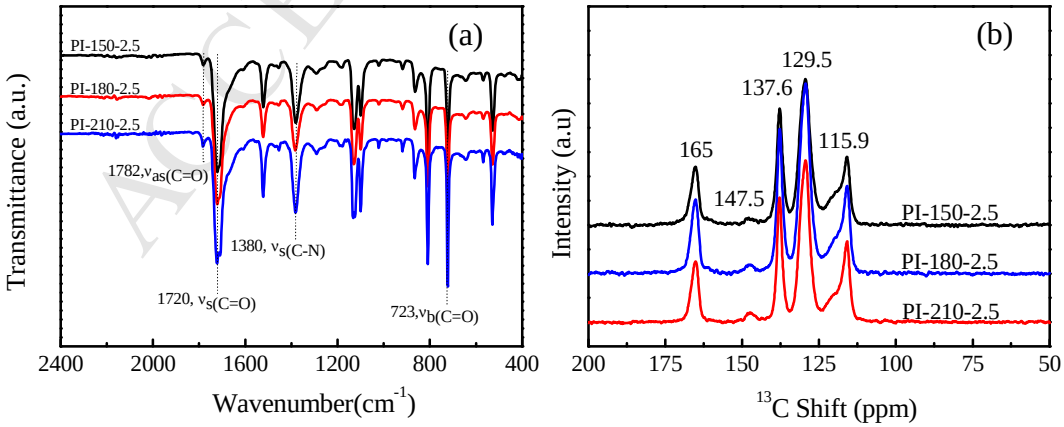

Fig. 1. (a) FTIR spectra and (b) ^{13}C NMR spectra of PI-150-2.5, PI-180-2.5 and PI-210-2.5.

Traditionally, a post-cure step is necessary to ensure full ring closure in the synthesis of polyimides.[24-26] However, the hydrothermal synthesis method in this work resulted in polyimide without post-curing, as was proven by the FTIR data shown in Fig. S1. It can be seen that the FTIR spectra of post-cured samples are identical to that of the as-synthesised samples, confirming complete imidisation of the polyimide obtained from the hydrothermal synthesis method. The successful synthesis of polyimides was further confirmed by the ^{13}C MAS NMR results shown in Fig. 1b. The peak at 165 ppm corresponds to the imide carbonyl carbon, the small peak at 147.5 ppm to the aromatic carbon connected to terminal amino group, the peak at 137.6 ppm to the non-protonated aromatic carbon of the bensimide group, and the peak at 129.5 ppm to protonated aromatic bensimide carbon, respectively. The peak at 115.9 ppm can be assigned to the N-substituted aromatic carbon and the protonated aromatic carbon of the N-substituted phenyl group. The NMR spectra match well with previously published results.[27]

Fig. 2a shows the XRD patterns of the polyimide samples synthesised at different temperatures. It can be seen that the crystallinity was increased at higher synthesis temperature as seen from the increased peak intensities. This is because higher improved hydrothermal synthesis temperature increases the system pressure, favouring crystallisation of the polyimides.[28] The average crystallite dimension or size of the coherent crystalline domain and lattice imperfections can be determined using the Williamson and Hall equation:[29, 30]

$$\beta cos\theta = 4\varepsilon sin\theta + 0.9\lambda/D$$

where β is the corrected integral width, ε is the microstrain ($\Delta d/d$, d: lattice-plane spacing), and D is the average size of crystallite domain. The above equation was applied to the six relatively strong peaks at approximately 14.2˚, 19.4˚, 21.2˚, 27.7˚, 30.5˚ and 36.2˚ two theta. By plotting $\beta cos\theta$ against $sin\theta$, an intercept ($0.9\lambda/D$) and a slope (4ε) that correlate with the

average size of crystallite domain and microstrain, respectively, were obtained. As can be seen from Figs. 2b-d, the plots gave a similar intercept, but very different slopes. The plot of the sample synthesised at 210 ^{o}C showed a smaller slope than the sample synthesised at 150 ^{o}C, indicating a smaller microstrain.

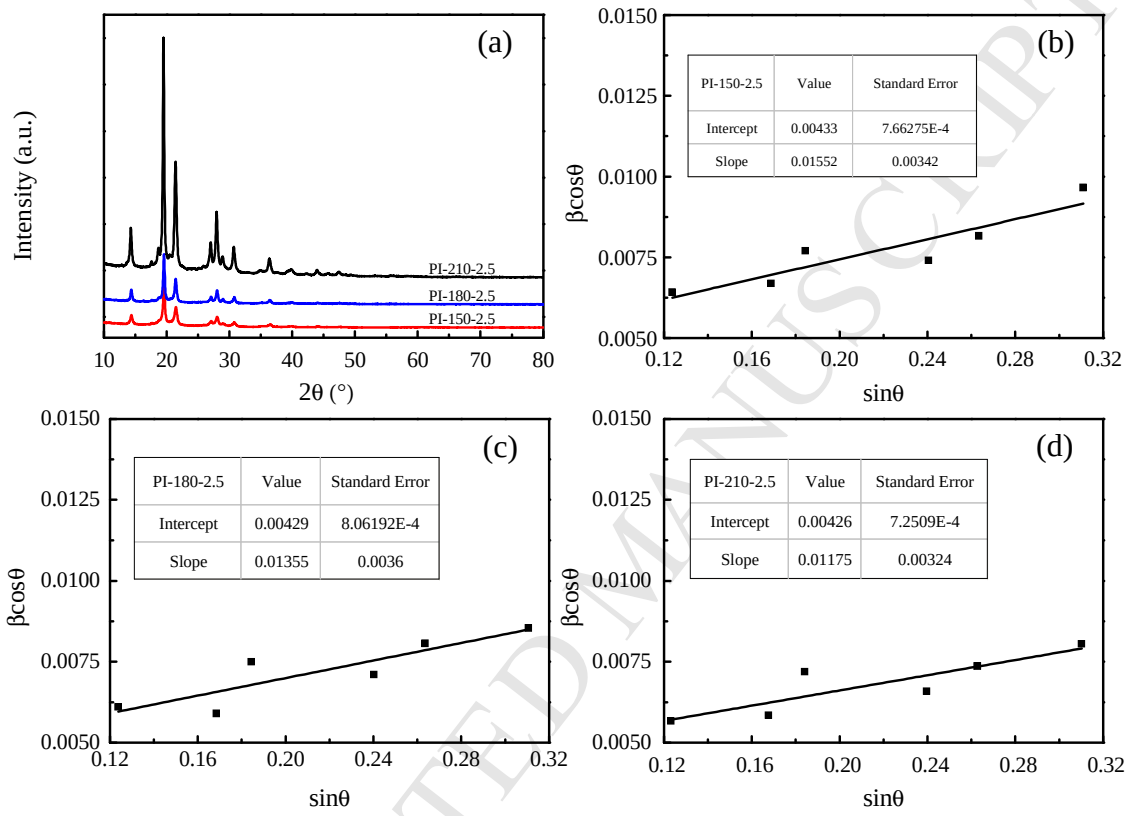

Fig. 2. (a) XRD patterns and (b-d) plots of the Williamson and Hall equation of as-synthesised samples (b) PI-150-2.5, (c) PI-180-2.5 and (d) PI-210-2.5.

Fig. 3 shows the FESEM images of samples PI-210-1.25, PI-210-2.5 and PI-210-5. All samples are in the form of micrometre-sized particles consisting of nanosheets as the primary particles. In addition, the primary particles became smaller as the reagent concentration increased, which is ascribed to increased nucleation density during the polymerisation reaction.[31] The PI-210-1.25 exhibited two-dimensional (2D) lamellar morphology (Fig. 3a), and the PI-210-2.5 and PI-210-5 synthesised at higher concentrations

presented three-dimensional (3D) interconnected microflower-like morphology composed from 2D nanosheets (Fig. 3b and c). The formation of the 3D microflowers is a result of the growth mechanism of spherulites.[32, 33] At low concentrations, the 2D lamellar structures were formed by polymer chains orienting perpendicularly to the nanosheet plane. At higher concentrations, fully developed 3D microflower-like structures were formed by the self-assembly of additional nanosheets via unidirectional growth and low angle branching. In energy storage systems, 3D structures have advantages over 2D structures, such as high contact area, novel physical properties, and structural stability during cycling.[34-36] Here, the 2D polyimide as the primary building block can be exposed as electroactive sites to sodium ions, while the 3D polyimide can present a shorter pathway for diffusion of sodium ions due to the interconnected nanosheet structure.

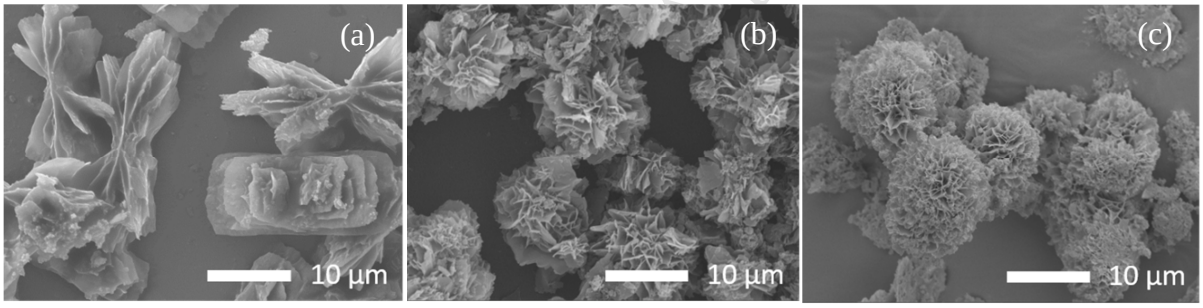

Fig. 3. FESEM images of (a) PI-210-1.25, (b) PI-210-2.5 and (c) PI-210-5.

Fig. S2 shows the nitrogen adsorption-desorption isotherms and the corresponding pore size distributions of PI-210-1.25, PI-210-2.5 and PI-210-5 synthesised using different concentrations of the reagents. As shown in Fig. S2a, all of the samples presented a type IV isotherm with a hysteresis loop, indicating the existence of the mesopores. The pore size distributions in Fig. S2b also confirmed that the samples had a mesoporous structure, and the sample PI-210-2.5 occupied a very wide mesopore distribution ranging from 4.5 nm to 40 nm. It can be seen from Table S1 that mesopores comprised a major proportion of the pore structure in all samples. Although PI-210-5 had the highest specific surface area, PI-210-2.5

occupied the largest mesopore volume of 0.2552 $cm^3 g^{-1}$. A large surface area in mesoporous materials can enhance the contact area between electrode materials and the electrolyte. A mesoporous structure can not only promote the infiltration of electrolyte to shorten the diffusion pathways for sodium ions, but also provide a large effective working interface for electrochemical reactions to decrease the electrochemical polarisation and improve the capacity utilisation and rate capability of the electrode.[37]

Fig. 4a shows the electrochemical impedance spectra of PI-150-2.5, PI-180-2.5 and PI-210-2.5. It can be seen that polyimides synthesised at 210 °C show smaller diameter of the semicircle in the medium frequency region than that of the other samples, indicating lower charge transfer resistance. The lower microstrain of PI-210-2.5 may enhance the ion transport in the material,[38, 39] leading to improved charge transfer at the interface between the electrode and electrolyte.[40] Fig. 4b shows the cycling performance of the PI-150-2.5, PI-180-2.5 and PI-210-2.5 at a current density of 25 mA g^{-1} between 0.005 and 3 V. As expected, the sample PI-210-2.5 achieved higher capacity and better cycling performance than PI-150-2.5 and PI-180-2.5. The superior cycling performance may be associated to the lower microstrain, which can cause less irreversible capacity loss.[41, 42] It should be noted that all the polyimide electrodes delivered an extremely high initial discharge capacity, which can be ascribed to the decomposition of electrolyte and the formation of a solid electrolyte interphase (SEI) at the low potential range. As is shown in Fig. S5, the formation and growth of SEI layer were evident from the increased size of the Nyquist semicircle of the cycled electrode in three-electrode cells in the initial few cycles.[43] After the 5^{th} cycle, the resistance almost stabilised.

Fig. 4c shows the cycling performance of PI-210-1.25, PI-210-2.5 and PI-210-5 at a current density of 25 mA g^{-1} between 0.005 and 3 V. It can be seen that PI-210-2.5 delivered the highest capacity of 125 mAh g^{-1} at the 100^{th} cycle, corresponding to approximately 68 %

of the theoretical capacity of 185 mAh g^{-1} according to the Equation 1. The coulombic efficiency of PI-210-2.5 reached 80 % at the 10th cycle and remained nearly 95 % at the 100th cycle as shown in Fig. S4. The weight ratio of carbon black for the preparation of organic electrodes is usually 30 wt% or even higher.[1, 6, 7, 15, 20-22] Considering 30 wt% of carbon black used during the polyimide electrode preparation, cycling performance of carbon black was also investigated at the same condition as shown in Fig. S3, which indicates that the capacity contribution (~11 mAh g^{-1}) from carbon black is negligible. Fig. 4d presents the rate performance of PI-210-1.25, PI-210-2.5 and PI-210-5 at different current densities. PI-210-2.5 achieved the highest capacity under the same current density, showing the best rate performance. Initial discharge capacities of 124, 90, 71, 59, 50, 43 mAh g^{-1} were achieved at current densities of 50, 100, 200, 500, 1000, 2000 mA g^{-1}, respectively. It should be pointed out that at a current density of 2000 mA g^{-1}, PI-210-2.5 delivered a discharge capacity of 43 mAh g^{-1}. In addition, a reversible discharge capacity of 123 mAh g^{-1} can be recovered after 5 additional cycles when the current density was reduced to 25 mA g^{-1}, demonstrating a good rate capability. The good rate performance of PI-210-2.5 can be explained by its open macroscopic structure exposing the electrode to the electrolyte, and mesoporous structure for enhanced electrolyte transport as well as effective interconnected structure.

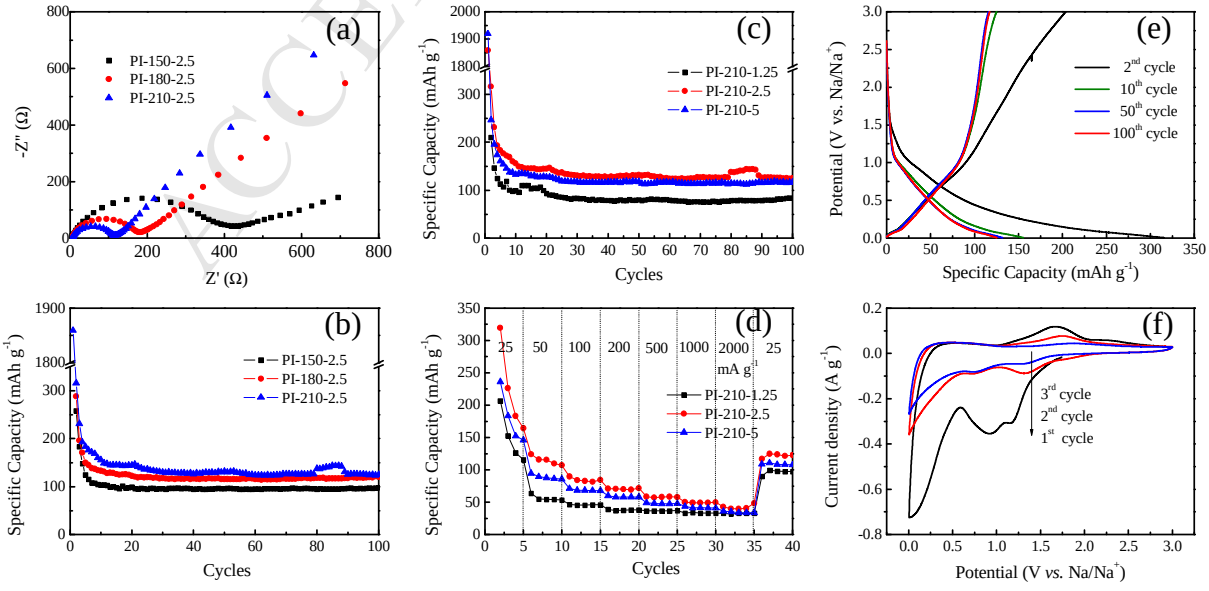

Fig. 4. (a) Nyquist plots of PI-150-2.5, PI-180-2.5 and PI-210-2.5 for the fresh cells, (b) cycling performance for PI-150-2.5, PI-180-2.5 and PI-210-2.5 synthesised under different temperatures, (c) cycling performance for PI-210-1.25, PI-210-2.5 and PI-210-5 synthesised at different reagent concentrations, (d) rate performance for PI-210-1.25, PI-210-2.5 and PI-210-5 from the second discharge capacity, (e) selected discharge and charge profiles for PI-210-2.5, and (f) CV curves at a scan rate of 0.2 mV s^{-1} for PI-210-2.5.

Selected discharge and charge profiles of PI-210-2.5 at a current density of 25 mA g^{-1} are shown in Fig. 4e. It can be seen that the capacity stabilised after the 10^{th} cycle. The discharge and charge profiles from the second cycle appeared very similar with sloping curves due to fast redox reactions.[22, 44, 45] Additionally, it can be found that the capacity was mainly from a discharge voltage below 1.5 V, indicating the suitability of this polyimide electrode as an anode for NIBs. Fig. 4f displays the CV curves of the polyimide electrodes between 0.005-3 V vs. Na/Na^+ at the scan rate of 0.2 mV s^{-1}. During the first cathodic scan, a strong broadened and split reduction peak between 0.5-1.5 V was observed. This peak became diminished in the next cycle. As a result, this peak may be due to the formation of a SEI layer along with the sodiation of the polyimide. During the reverse anodic scan, there was a broad peak between 1-2 V, corresponding to the desodiation of the sodiated polyimide. In the next scan, two cathodic peaks appeared at potentials of 0.75 and 1.25 V, likely corresponding to the sodiation of the carbonyls into radical anions and dianions.[22] These two close redox peaks with only a slightly positive shift can be also seen during subsequent scans, indicating a multiple and fast electron transfer reaction as well as good reversibility. The CV results were consistent with the discharge and charge observations.

Fig. 5 shows typical FTIR spectra of the PI-210-2.5 electrodes discharged to 0.005 V and recharged to 3 V. As discussed above, the signals at 1720 and 723 cm^{-1} were attributed to

v_s(imide C=O) and δ(imide C=O) of the active material polyimide. It was found that the peak of the δ(imide C=O) decreased in intensity when the electrode was discharged to 0.005 V, indicating reduction of the carbonyl groups. In addition, the peak due to v_s(imide C=O) gradually shifted from 1720 cm^{-1} to 1726 cm^{-1}, due to formation of sodium enolate O–C–O–Na.[22] When the electrode was recharged to 3 V, the intensity of the δ(imide C=O) peak gradually recovered, demonstrating the recovery of the carbonyl groups due to desodiation. After discharging to 1 V where the CV curve shows a huge reduction peak, two new peaks at 1655 and 1588 cm^{-1} appeared and remained after recharging, which may be due to the SEI layer.[46] Additionally, during the discharge and charge processes, the peak at 1518 cm^{-1} attributed to the stretching vibration of C=C in phenyl rings was almost unchanged, suggesting that the unsaturated double carbon bond does not actively participate in sodium-ion storage. The FTIR results also match well with the CV observation (Fig. 4f) that there was sodiation of the carbonyls into radical anion and dianion during the redox reaction. When combining analysis of the CV results and the reversible discharge-charge capacities (125 mAh g^{-1} at the 100th cycle), the redox mechanism of the PMDA-based polyimide can be illustrated as a two-step enolisation reaction with reversible insertion of two sodium ions as shown in scheme 1.

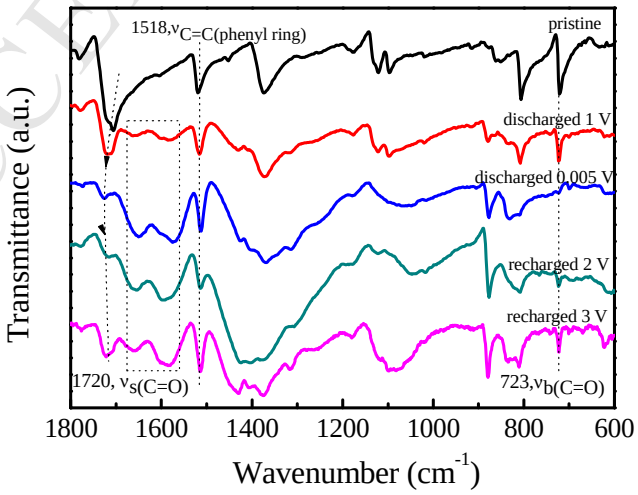

Fig. 5. FTIR spectra of the polyimide electrodes at different discharged and charged states.

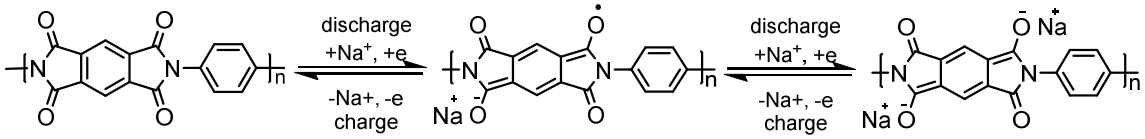

Scheme 1. Possible discharge and charge mechanism for the PMDA-based polyimide in a NIB.

4. Conclusion

In this study, a one-pot hydrothermal method was used to prepare polyimides with controllable hierarchical mesoporous structure constructed from nanosheets. A microflower-like polyimide with high degree of crystallinity and large mesopore volume can be obtained by adjusting synthesis temperatures and reagent concentrations to achieve higher capacity and superior performance. As an anode material in sodium-ion batteries (NIBs), the PMDA-based polyimide experienced a two-step enolisation reaction with reversible insertion of two sodium ions during the redox electrochemical reaction. This polyimide electrode can be considered as promising for organic sodium-ion batteries with its capacity mainly contributed below 1.5 V and a high reversible capacity of 125 mAh g^{-1} at the 100^{th} cycle. This nontoxic polymer is inexpensive and simple to synthesise, and can therefore fulfil the needs for large-scale battery applications. Overall, this study provides a new method to improve the electrochemical performance of organic electrodes via adjusting the structure and morphology.

Conflict of interest

None.

Acknowledgements

This research was supported by The Australian Research Council (ARC) under the ARC Laureate Fellowship program (FL170100101). QZ thanks the International Postgraduate Research Scholarship funded by the Australian Government and the UQ Centennial Scholarship. QZ also thanks Jinli Tan from Changsha Research Institute of Mining and Metallurgy, Co. Ltd. Hunan, China. Ashok Kumar Nanjundan from the School of Chemical Engineering, The University of Queensland, Australia, is acknowledged for his valuable discussion. The authors gratefully acknowledge the facilities, scientific and technical assistance of the Australian Microscopy and Microanalysis Research Facility at the UQ Centre for Microscopy and Microanalysis.

References

[1] F. Wan, X.L. Wu, J.Z. Guo, J.Y. Li, J.P. Zhang, L. Niu, R.S. Wang, Nanoeffects promote the electrochemical properties of organic $Na_2C_8H_4O_4$ as anode material for sodium-ion batteries, Nano Energy 13 (2015) 450-457.

[2] C. Shi, K. Xiang, Y. Zhu, X. Chen, W. Zhou, H. Chen, Preparation and electrochemical properties of nanocable-like Nb_2O_5/surface-modified carbon nanotubes composites for anode materials in lithium ion batteries, Electrochim. Acta 246 (2017) 1088-1096.

[3] M. Armand, J.M. Tarascon, Building better batteries, Nature 451 (2008) 652-657.

[4] V. Palomares, P. Serras, I. Villaluenga, K.B. Hueso, J. Carretero-González, T. Rojo, Na-ion batteries, recent advances and present challenges to become low cost energy storage systems, Energy Environ. Sci. 5 (2012) 5884-5901.

[5] K. Saravanan, C.W. Mason, A. Rudola, K.H. Wong, P. Balaya, The first report on excellent cycling stability and superior rate capability of $Na_3V_2(PO_4)_3$ for sodium ion batteries, Adv. Energy Mater. 3 (2013) 444-450.

[6] C. Wang, Y. Xu, Y. Fang, M. Zhou, L. Liang, S. Singh, H. Zhao, A. Schober, Y. Lei, Extended π-conjugated system for fast-charge and -discharge sodium-ion batteries, J. Am. Chem. Soc. 137 (2015) 3124-3130.

[7] A. Abouimrane, W. Weng, H. Eltayeb, Y. Cui, J. Niklas, O. Poluektov, K. Amine, Sodium insertion in carboxylate based materials and their application in 3.6 V full sodium cells, Energy Environ. Sci. 5 (2012) 9632-9638.

[8] J.J. Braconnier, C. Delmas, C. Fouassier, P. Hagenmuller, Comportement electrochimique des phases Na_xCoO_2, Mater. Res. Bull. 15 (1980) 1797-1804.

[9] M.M. Doeff, M.Y. Peng, Y. Ma, L.C. De Jonghe, Orthorhombic Na_xMnO_2 as a cathode material for secondary sodium and lithium polymer batteries, J. Electrochem. Soc. 141 (1994) L145-L147.

[10] J.M. Paulsen, J.R. Dahn, Studies of the layered manganese bronzes, $Na_{2/3}[Mn_{1-x}M_x]O_2$ with M = Co, Ni, Li, and $Li_{2/3}[Mn_{1-x}M_x]O_2$ prepared by ion-exchange, Solid State Ion. 126 (1999) 3-24.

[11] B.L. Ellis, W.R.M. Makahnouk, Y. Makimura, K. Toghill, L.F. Nazar, A multifunctional 3.5 V iron-based phosphate cathode for rechargeable batteries, Nat. Mater. 6 (2007) 749-753.

[12] P. Moreau, D. Guyomard, J. Gaubicher, F. Boucher, Structure and stability of sodium intercalated phases in olivine $FePO_4$, Chem. Mater. 22 (2010) 4126-4128.

[13] M.D. Slater, D. Kim, E. Lee, C.S. Johnson, Sodium-ion batteries, Adv. Funct. Mater. 23 (2013) 947-958.

[14] Z. Li, Z. Jian, X. Wang, I. A. Rodríguez-Pérez, C. Bommier, X. Ji, Hard carbon anodes of sodium-ion batteries: undervalued rate capability, Chem. Commun., 2017, 53, 2610-2613.

[15] H. Banda, D. Damien, K. Nagarajan, A. Raj, M. Hariharan, M.M. Shaijumon, Twisted perylene diimides with tunable redox properties for organic sodium-ion batteries, Adv. Energy Mater. 7 (2017) 1701316.

[16] Z. Song, H. Zhou, Towards sustainable and versatile energy storage devices: an overview of organic electrode materials, Energy Environ. Sci. 6 (2013) 2280-2301.

[17] Q. Zhao, Y. Lu, J. Chen, Advanced organic electrode materials for rechargeable sodium-ion batteries, Adv. Energy Mater. 7 (2017) 1601792.

[18] B. Häupler, A. Wild, U.S. Schubert, Carbonyls: powerful organic materials for secondary batteries, Adv. Energy Mater. 5 (2015) 1402034.

[19] M.K. Ghosh, K.L. Mittal, Polyimides: fundamentals and applications, Marcel Dekker, New York, 1996.

[20] F. Xu, J. Xia, W. Shi, Anthraquinone-based polyimide cathodes for sodium secondary batteries, Electrochem. Commun. 60 (2015) 117-120.

[21] H. Banda, D. Damien, K. Nagarajan, M. Hariharan, M.M. Shaijumon, A polyimide based all-organic sodium ion battery, J. Mater. Chem. A 3 (2015) 10453-10458.

[22] H.G. Wang, S. Yuan, D.L. Ma, X.L. Huang, F.L. Meng, X.B. Zhang, Tailored aromatic carbonyl derivative polyimides for high-power and long-cycle sodium-organic batteries, Adv. Energy Mater. 4 (2014) 1301651.

[23] B. Baumgartner, M.J. Bojdys, M.M. Unterlass, Geomimetics for green polymer synthesis: highly ordered polyimides via hydrothermal techniques, Poly. Chem. 5 (2014) 3771-3776.

[24] J.H. Jou, P.T. Huang, Effect of thermal curing on the structures and properties of aromatic polyimide films, Macromolecules 24 (1991) 3796-3803.

[25] J.J. Bergmeister, L.T. Taylor, Synthetic strategies in the formation of iron-modified polyimide films, Chem. Mater. 4 (1992) 729-737.

[26] B.W. Jo, K.H. Ahn, S.J. Lee, Effect of thermal history during drying and curing process on the chain orientation of rod-shaped polyimide, Polymer 55 (2014) 5829-5836.

[27] T. Brock, D.C. Sherrington, J. Swindell, Synthesis and characterisation of porous particulate polyimides, J. Mater. Chem. 4 (1994) 229-236.

[28] K. Takizawa, H. Fukudome, Y. Kozaki, S. Ando, Pressure-induced changes in crystalline structures of polyimides analyzed by wide-angle x-ray diffraction at high pressures, Macromolecules 47 (2014) 3951-3958.

[29] V.D. Mote, Y. Purushotham, B.N. Dole, Williamson-Hall analysis in estimation of lattice strain in nanometer-sized ZnO particles, J. Theor. Appl. Phys. 6 (2012) 6.

[30] G.K. Williamson, W.H. Hall, X-ray line broadening from filed aluminium and wolfram, Acta Metall. 1 (1953) 22-31.

[31] D.R. Lloyd, G.B. Lim, Microporous membrane formation via thermally-induced phase separation. VII. Effect of dilution, cooling rate, and nucleating agent addition on morphology, J. Membr. Sci. 79 (1993) 27-34.

[32] A. Keller, Polymer single crystals, Polymer 3 (1962) 393-421.

[33] L. Gránásy, T. Pusztai, G. Tegze, J.A. Warren, J.F. Douglas, Growth and form of spherulites, Phys. Rev. E 72 (2005) 011605.

[34] S. Li, Y. Dong, L. Xu, X. Xu, L. He, L. Mai, Effect of carbon matrix dimensions on the electrochemical properties of $Na_3V_2(PO_4)_3$ nanograins for high-performance symmetric sodium-ion batteries, Adv. Mater. 26 (2014) 3545-3553.

[35] S.H. Choi, Y.N. Ko, J.K. Lee, Y.C. Kang, 3D MoS_2-graphene microspheres consisting of multiple nanospheres with superior sodium ion storage properties, Adv. Funct. Mater. 25 (2015) 1780-1788.

[36] Y. Liu, H. Kang, L. Jiao, C. Chen, K. Cao, Y. Wang, H. Yuan, Exfoliated-SnS_2 restacked on graphene as a high-capacity, high-rate, and long-cycle life anode for sodium ion batteries, Nanoscale 7 (2015) 1325-1332.

[37] Y. Fang, L. Xiao, J. Qian, X. Ai, H. Yang, Y. Cao, Mesoporous amorphous $FePO_4$ nanospheres as high-performance cathode material for sodium-ion batteries, Nano Lett. 14 (2014) 3539-3543.

[38] J. Jiang, W. Shen, J. L. Hertz, Structure and ionic conductivity of nanoscale gadolinia-doped ceria thin films, Solid State Ionics 249-250 (2013) 139-143.

[39] N. Schichtel, C. Korte, D. Hesse, N. Zakharov, B. Butz, D. Gerthsen, J. Janek, On the influence of strain on ion transport: microstructure and ionic conductivity of nanoscale YSZ|Sc_2O_3 multilayers, Phys. Chem. Chem. Phys. 12 (2010) 14596-14608.

[40] M. Watanabe, T. Endo, A. Nishimoto, K. Miura, M. Yanagida, High ionic conductivity and electrode interface properties of polymer electrolytes based on high molecular weight branched polyether, J. Power Sources 81-82 (1999) 786-789.

[41] C. R. Fell, D. Qian, K. J. Carroll, M. Chi, J. L. Jones, Y. S. Meng, Correlation between oxygen vacancy, microstrain, and cation distribution in lithium-excess layered oxides during the first electrochemical cycle, Chem. Mater. 25 (2013) 1621-1629.

[42] R. Robert, P. Novák, Structural changes and microstrain generated on $LiNi_{0.80}Co_{0.15}Al_{0.05}O_2$ during cycling: effects on the electrochemical performance, J. Electrochem. Soc. 162 (2015) A1823-A1828.

[43] C. Wang, A. J. Appleby, F. E. Little, Irreversible capacities of graphite anode for lithium-ion batteries, J. Electroanal. Chem. 519 (2002) 9-17.

[44] X. Han, C. Chang, L. Yuan, T. Sun, J. Sun, Aromatic carbonyl derivative polymers as high-performance Li-ion storage materials, Adv. Mater. 19 (2007) 1616-1621.

[45] Z. Song, H. Zhan, Y. Zhou, Polyimides: Promising energy-storage materials, Angew. Chem. 122 (2010) 8622-8626.

[46] H.G. Wang, S. Yuan, Z. Si, X.B. Zhang, Multi-ring aromatic carbonyl compounds enabling high capacity and stable performance of sodium organic batteries, Energy Environ. Sci. 8 (2015) 3160-3165.

Highlights

- Pyromellitic dianhydride-based polyimides were prepared by one-step hydrothermal method.
- Pyromellitic dianhydride-based polyimides show promise as anode for sodium-ion batteries.
- The electrochemical performance of polyimides can be affected by the crystallinity and morphology.
- This polyimide electrode achieved a capacity of 125 mAh g^{-1} at 25 mA g^{-1} and 43 mAh g^{-1} at 2 A g^{-1}.
- It experienced two-step enolisation reaction with reversible insertion of two sodium ions.